

Contents lists available at ScienceDirect

## Journal of Alloys and Compounds

journal homepage: www.elsevier.com/locate/jalcom



# Morphology-controlled synthesis of MoS<sub>2</sub> nanostructures with different lithium storage properties



Xiwen Wang, Zhian Zhang\*, Yaqiong Chen, Yaohui Qu, Yanqing Lai, Jie Li\*

School of Metallurgy and Environment, Central South University, Changsha 410083, China

#### ARTICLE INFO

Article history:
Received 16 November 2013
Received in revised form 19 February 2014
Accepted 20 February 2014
Available online 28 February 2014

Keywords: Molybdenum disulfide Nanospheres Nanoribbons Nanoparticles Lithium-ion batteries

#### ABSTRACT

A one-step hydrothermal process was employed to prepare a series of  $MoS_2$  nanostructures via simply altering the surfactant as soft template and hydrothermal reaction temperature. Three kinds of  $MoS_2$  nanostructures (three-dimensional (3D) hierarchical nanospheres, one-dimensional (1D) nanoribbons, and large aggregated nanoparticles) were successfully achieved and investigated well by X-ray diffraction (XRD), field emission scanning electron microscopy (FESEM), high resolution transmission electron microscopy (HRTEM), and Brunauer–Emmett–Teller analysis (BET). Electrochemical tests reveal that these  $MoS_2$  samples could deliver high initial discharge capacities (higher than 1050.0 mA h g<sup>-1</sup>), but various cycling performances. The hierarchical  $MoS_2$  nanospheres assembled by sheet-like subunits show the highest specific capacity of 1355.1 mA h g<sup>-1</sup>, and 66.8% of which can be retained after 50 cycles. The good lithium storage property of hierarchical  $MoS_2$  nanospheres can be attributed to the higher electrolyte/ $MoS_2$  contact area and stable 3D layered structure.

© 2014 Elsevier B.V. All rights reserved.

#### 1. Introduction

Li-ion batteries (LIBs) are the main power sources for portable electronic devices and hybrid electric vehicles [1–3]. Graphite has been commonly used as anode materials in commercial LIBs. However, the limited theoretical capacity of graphite (372 mA h g<sup>-1</sup>) could not meet the requirement of future energy storage system [4]. As one type of two-dimensional (2D) layered materials, transition metal disulfides (TMDs) MS<sub>2</sub> such as MoS<sub>2</sub> [5], SnS<sub>2</sub> [6], WS<sub>2</sub> [7] and ZrS<sub>2</sub> [8] have been exploited as the novel anode materials of LIBs owing to their graphene-like structure, in which atoms are covalently bonded within the individual layers that are bound by weak van der Waals force. This graphene-like structure enables the convenient insertion and extraction of Li<sup>+</sup> ions.

Among the graphene analogous TMDs,  $MoS_2$  is found to be one of the most promising anode material for LIBs because there is a 4-electron transfer reaction occurring at lower potential during the charge/discharge process achieving high capacities up to  $1000~\text{mA}~\text{h g}^{-1}$ . However, the rapid capacity fading and poor rate performance result in its limited practical application due to the gel-like polymeric layer formed by the reaction between the lithiation product  $\text{Li}_2S$  and electrolyte, which will prevent the successive lithiation/delithiation reaction [9–12]. An extensive used

strategy to address this issue is to design different nanostructure. Du et al. reported the synthesis of restacked MoS<sub>2</sub> nanostructures that gave a high specific capacity of 750 mA h g<sup>-1</sup> after 50 cycles, while the raw MoS<sub>2</sub> faded to 226 mA h g<sup>-1</sup> [13]. MoS<sub>2</sub> nanorods prepared by a sulfidation method demonstrated an excellent cycling stability with a high capacity of 621 mA h  $\rm g^{-1}$  after 80 cycles [14]. Other MoS<sub>2</sub> nanostructures including nanosheets [15], nanoflowers [16], nanoplates [17], nanowalls [18] and hollow nanoparticles [19] have also been reported as LIBs anode materials. Although there are many reports about MoS<sub>2</sub> nanostructures with improved lithium storage properties, most of them only focused on one type of MoS<sub>2</sub> nanostructures. The morphology could have an important impact on the surface area, active site and ion kinetics of materials, which could effectively influence its electrochemical performance [20,21]. Therefore, it is necessary to investigate the morphology-depending electrochemical performance of various MoS<sub>2</sub> nanostructures.

Meanwhile, even though various synthetic methods have been developed, it is still a challenge to achieve the shape-controlled MoS<sub>2</sub> nanostructure through a facile and environmentally friendly method. Among all synthesis strategies, the surfactant-assisted hydrothermal method is considered to be a direct reaction route to control both the morphology and phase of inorganic materials. MnWO<sub>4</sub> [22], Mn<sub>2</sub>O<sub>3</sub> [23] and NiS<sub>x</sub> [24] nanostructures have been prepared by a hydrothermal process in presence of different surfactant.

<sup>\*</sup> Corresponding authors. Tel./fax: +86 731 88830649. E-mail address: zza75@163.com (Z. Zhang).

In this work, we report a facile approach to prepare MoS<sub>2</sub> nanostructures with different morphologies and sizes via a hydrothermal method by controlling the added surfactant and hydrothermal reaction temperature. MoS<sub>2</sub> nanostructures with nanospheres, nanoribbons and nanoparticles morphologies have been successfully synthesized. The electrochemical properties of three kinds of as-prepared MoS<sub>2</sub> samples were investigated as anode materials for LIBs. Among these samples, the MoS<sub>2</sub> hierarchical nanospheres with high specific surface area and stable structure show the best cycling stability and rate performance.

#### 2. Experiment

#### 2.1. Preparation of MoS<sub>2</sub> nanostructures

MoS $_2$  nanoribbons (NSs) were fabricated as the following procedures: 0.5 g sodium molybdate (Na $_2$ MoO $_4$ ·2H $_2$ O) and 0.6 g thioacetamide (TAA) were dissolved in 40 mL de-ionized water under vigorous stirring. After stirring for 15 min, 0.14 g polyvinyl pyrrolidone (PVP) was added to the above solution. Then, the transparent solution was transferred into a 50 mL Teflon-lined stainless steel autoclave. The autoclave was sealed and heated to 200 °C with a heating rate of 5 °C min $^{-1}$  and held for 24 h. After that, the autoclave was cooled to room temperature. The black products deposited at the bottom were washed by centrifugation for three times using de-ionized water and dried in oven at 60 °C for 12 h.

The  $MoS_2$  nanoribbons (NRs) were synthesized by the similar procedures above except that 0.4 g poly(ethylene glycol octylphenol ether) (Triton X-100) was used to substitute PVP in reaction solution.

For the synthesis of  $MoS_2$  nanoparticles (NPs), both the surfactant and hydrothermal reaction temperature were changed. 0.54 g cetyltrimethyl ammonium bromide (CTAB) was added into a mixed solution of  $Na_2MoO_4$  and TAA. The mixture was hydrothermally treated at 160 °C for 24 h.

#### 2.2. Materials characterization

The crystal structure of samples was measured by X-ray diffractometer (XRD, Rigaku D/max 2550VB+) from 10° to 80° with Cu K $\alpha$  radiation ( $\lambda$  = 1.54056 Å). The product morphology was characterized by scanning electron microscope (SEM, Nova NanoSEM 230), transmission electron microscope (TEM, Tecnai G2 20ST). Nitrogen adsorption/desorption measurements were performed by using Quantachrome instrument (Quabrasorb SI-3MP) at 77 K.

#### 2.3. Electrochemical measurements

The electrochemical characterization was carried out using a CR-2025 type coin cell with a lithium metal sheet as the counter and reference electrode and a Celgard 2400 film as separator. The working electrode was prepared by casting a slurry consisted of 80 wt% active materials, 10 wt% acetylene black and 10 wt% polyvinylidene fluoride (PVDF) in N-methyl pyrrolidinone (NMP) on a copper foil. Then, the slurry was dried at 100 °C under vacuum overnight. The test cells were assembled in an argon-filled glove box (Universal 2440/750). The electrolyte was 1.0 M LiPF $_6$  solution in a 1:1:1 v/v mixture of ethylene carbonate (EC), ethyl methyl carbonate (EMC) and diethyl carbonate (DMC).

The charge/discharge tests were carried out in potential window of 0.01–3.0 V with a LAND CT2001A battery-testing system. The EIS were measured in the frequency range of 100 k–0.1 Hz with AC voltage amplitude of 5 mV at open-circuit voltage on PARSTAT 2273 electrochemical measurement system.

#### 3. Results and discussion

#### 3.1. Structure and morphology characterizations

Fig. 1 shows the XRD patterns of as-prepared  $MoS_2$  nanostructures. All diffraction lines of three samples can be indexed to hexagonal  $2H-MoS_2$  (JCPDS No. 37-1492), which belongs to the space group P63/mmc (No. 194). Intensive diffraction peaks at  $2\theta = 34.5^{\circ}$ ,  $42.0^{\circ}$  and  $59.2^{\circ}$  which correspond to (100), (103) and (110) planes of  $MoS_2$ , could be observed in XRD patterns of three samples. The intense peaks of  $MoS_2$  NPs at  $14.0^{\circ}$ , corresponding to the (002) reflection, indicates a well-stacked layered structure with a much larger d-spacing (0.62 nm) than natural graphite (0.34 nm). The  $MoS_2$  NRs exhibit a broadened and shortened (002) peaks  $(2\theta = 12.5^{\circ})$  than  $MoS_2$  NPs, suggesting a smaller crystallite size and a less number of layers in direction of the z-axis per-

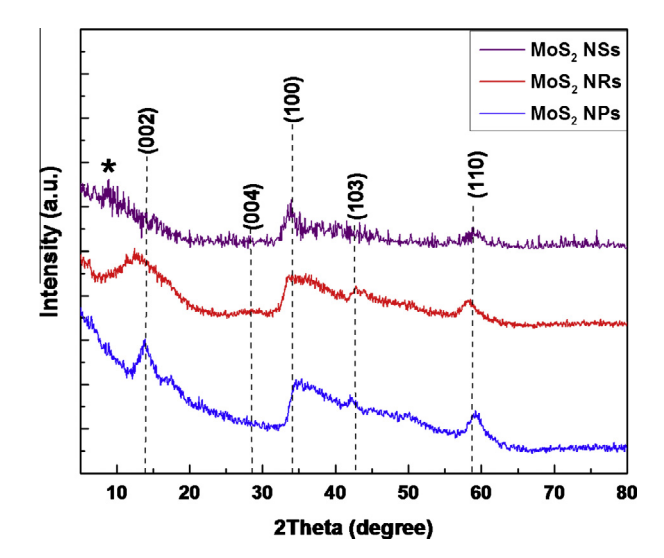


Fig. 1. XRD patterns of MoS<sub>2</sub> nanospheres, nanorobbins and nanoparticles.

pendicular to the atomic layers [11]. The (002) reflection even could not be observed in the XRD pattern of MoS<sub>2</sub> NSs, implying that this material may consist of five or less graphene-like MoS<sub>2</sub> layers [17]. A weak peak at  $8.5^{\circ}$  can be attributed to the diffraction of adjacent few-layered MoS<sub>2</sub> sheets. By using the Bragg equation, the interlayer distance of MoS<sub>2</sub> NRs and NSs are calculated to 0.69 and 0.98 nm respectively, providing a larger space for Li ions intercalation [25].

Morphologies of all MoS<sub>2</sub> nanostructures were examined with FESEM. Fig. 2a and b shows that the 3D MoS<sub>2</sub> NSs are in diameters of 600–900 nm and composed of the sheet-like subunits. The MoS<sub>2</sub> nanosheets could form MoS<sub>2</sub> nanoflakes and then MoS<sub>2</sub> nanoflakes aggregate to form the loose cauliflower-like architectures, which are similar to other reported 3D MoS<sub>2</sub> microspheres [18,26,27]. As shown in Fig. 2c and d, the MoS<sub>2</sub> NRs demonstrate a one-dimensional rod or ribbon shape with a width of 200–300 nm and a length up to several micrometers. It is noteworthy that the MoS<sub>2</sub> NRs exhibit a relatively smooth surface. To our best knowledge, the one-pot hydrothermal synthesis of 1D MoS<sub>2</sub> nanostructures has not been reported yet. Fig. 2e illustrates that the spherical MoS<sub>2</sub> NPs do not exhibit a good dispersions. The higher magnification FESEM (Fig. 2f) shows these particles are with a relatively uniform size of 600 nm and possess quite rough surfaces.

In order to further investigate structural information of three  $MoS_2$  samples, HRTEM and selected area electron diffraction (SAED) are presented in Fig. 3. It can be obviously seen from Fig. 3a and b that the  $MoS_2$  NSs and NRs consist of few-layered  $MoS_2$  sheets in random orientation. For  $MoS_2$  NSs and NRs, the interlayer distance of (002) plane measured from HRTEM images are 0.69 and 0.98 nm respectively, which coincide with the results from XRD analysis.  $MoS_2$  (002) planes do not stack together in the  $MoS_2$  NSs, confirming the absence of the (002) reflection in XRD pattern. For the  $MoS_2$  NPs in Fig. 3c, a well-layered structure with  $d_{(002)}$  spacing of 0.62 nm is observed, in good agreement with previous XRD results. More than 5 layers bond together tightly by van der Waals force to form thin sheets which then curl up to sphere-like particles. The SAED in inset of Fig. 3 reveal that the all three  $MoS_2$  nanostructures are weakly crystalline.

To characterize the specific surface area of three  $MoS_2$  nanostructures,  $N_2$  adsorption–desorption analysis were performed using Brunauer–Emmett–Teller (BET) method. Fig. 4 shows the  $N_2$  adsorption–desorption isotherms of these samples, and the insets exhibit the corresponding pore size distribution by Barrett– Joyner–Halenda (BJH) method. The isotherm curves of three

### Download English Version:

# https://daneshyari.com/en/article/1611311

Download Persian Version:

https://daneshyari.com/article/1611311

Daneshyari.com